Materials Research Proceedings 28 (2023) 1491-1502 https://doi.org/10.21741/9781644902479-161

ESAFORM 2021 cup drawing benchmark of an Al alloy: Critical follow up analysis of its potentials

OLIVEIRA Marta C.[1,a], CAZACU Oana[2,b], REVIL-BAUDARD Benoit[2,c], NETO Diogo M.[1,d], FROHN-SÖRENSEN Peter[3,e], MA Jun[4,f], LIU Wencheng[5,g], CRUZ Daniel J.[6,h], SANTOS Abel D.[6,i], VAN BAEL Albert[7,j], GHIABAKLOO Hadi[7,k] and HABRAKEN Anne M.[8,l *]

[1]CEMMPRE, Department of Mechanical Engineering, University of Coimbra, Polo II, Pinhal de Marrocos, 3030-788 Coimbra, Portugal

[2]Department of Mechanical and Aerospace Engineering, University of Florida, REEF, 1350N. Poquito Rd, Shalimar, FL 32579, USA

[3]Forming Technology (UTS), Institute of Production Technologies, University of Siegen, Breite Strasse, 11, 57076 Siegen, Germany

[4]Department of Mechanical and Industrial Engineering, Norwegian University of Science and Technology, 7491 Trondheim, Norway

[5]School of Civil Aviation, Northwestern Polytechnical University, Taicang 215400, China

[6]Institute of Science and Innovation in Mechanical and Industrial Engineering (INEGI), R. Dr. Roberto Frias 400, 4200-465 Porto, Portugal

[7]Department of Materials Engineering, Katholieke Universiteit Leuven, Kasteelpark Arenberg 44- box 2450, 3001 Leuven, Belgium

[8]ArGEnCo department, University of Liege, 9 Allée de la Découverte, 4000 Liège, Belgium

[a] marta.oliveira, [b]cazacu@reef.ufl.edu, [c]revil@ufl.edu, [d]diogo.neto@dem.uc.pt, [e]peter.frohn@uni-siegen.de, [f]jun.ma@ntnu.no, [g]wencheng.liu@usst.edu.cn, [h]dcruz@inegi.up.pt, [i]abel@fe.up.pt, [j]albert.vanbael@kuleuven.be, [k]ghiabakloo@gmail.com, [l]anne.habraken@uliege.be

Keywords: Benchmark, 6016-T4, Deep Drawing Modelling, Thickness Prediction, Ironing Force Prediction, Plastic Anisotropic Models

Abstract. The 1st ESAFORM Benchmark, called EXACT [1], enabled an in-depth study of the factors that contribute to the accuracy of predictions and efficiency of finite element (FE) simulations of deep drawing of a cup from AA 6016-T4 sheet through the joint work of 11 teams. FE analyses were conducted with elasto-plastic models or crystal plasticity approaches using commercial or academic FE codes. This paper reminds the content of EXACT benchmark and gives new results that highlight the importance of the tool stiffness and various contact conditions to predict the ironing forces and the thickness distribution along the cup wall. The use of the Benchmark experimental data and virtual tests performed with DAMASK crystal plasticity code to identify and validate a two-surface kinematic hardening model based on Yoshida and Uemori approach is also discussed.

Materials Research Proceedings 28 (2023) 1491-1502 https://doi.org/10.21741/9781644902479-161

Introduction

Hereafter, the work performed within ESAFORM 2021 benchmark is described and the structure and content of the quite extensive article (96 pages) [1] are reminded. Indeed, this detailed paper provides both theoretical equations and details on the identification methodologies, before the analysis of the FE results *versus* experiments. As pointed out in the next section, some discrepancies between measurements and predictions justify further investigations and the current article summarizes the ongoing activities around all the gathered data.

ESAFORM 2021 Benchmark consisted of a cup drawing process of a 1 mm thick AA 6016-T4 sheet with a strong cube component (52% volume fraction of grains). As shown in Fig. 1, the main goal is to accurately predict the punch force-displacement curve, the earing profile, the thickness distribution and the wall height. Another objective was to provide the dataset necessary to identify advanced models, both elasto-plastic macroscopic models or models accounting for the behavior of the constituent grains. Mechanical characterization tests and texture measurements post tests were also performed, including measurements of the texture of the fully-drawn cup (see Fig. 1)

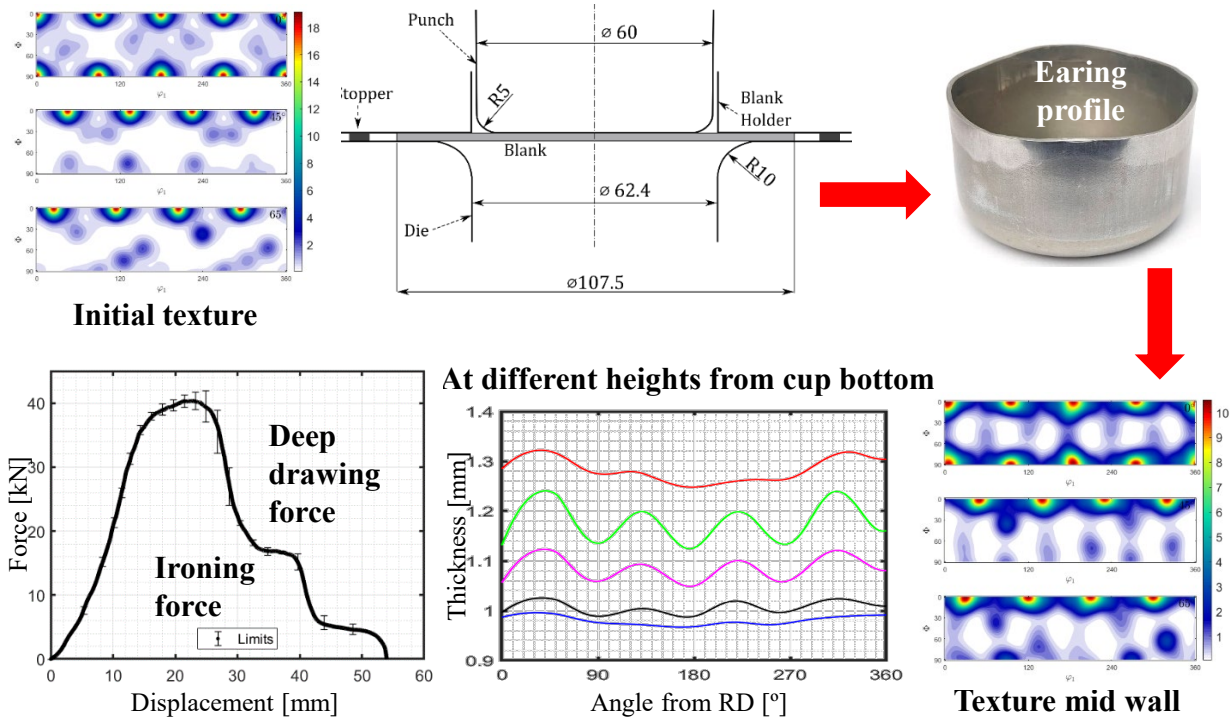

Fig. 1. Cup drawing of a circular blank (Φ =107.5mm) of AA 6016 sheet, adapted from [1].

Specifically, cup drawing tests done at University of Porto (UPorto) were complemented with extensive mechanical characterization by 2 independent teams: tensile tests in 7 orientations (true stress-strain curves and Lankford coefficients, obtained from several repeats of any given test, measured at Tokyo University of Agriculture and Technology (TUAT), and at the University of Aveiro (UA)), biaxial tests in TUAT, shear and reverse shear tests in UA and in the University of Liege (ULiege). For a detailed discussion of testing procedures and experimental errors see [1].

Finally, the initial texture and the one present after forming in the middle and at the top of the cup were measured at UA from coupons taken in the rolling direction (RD), 45° and 90° to the RD. The benchmark results (earing, wall height, thickness distribution, deep drawing, and ironing forces) were measured by UPorto (see [1]).

Eleven institutions participated using either commercial codes with built-in models or their implementation of other models in ABAQUS implicit or explicit, LS-DYNA, MSC.MARC, PAMSTAMP or academic FE Softwares (DD3IMP from Coimbra University (UCoimbra) or Lagamine from University of Liege (ULiege)). Some participants used various models.

The organization of the result presentation in article [1] is shown in Fig. 2. After describing the experimental tests, and a general discussion on friction effects, the choices made by the participants concerning material description, finite element models and FE type were described. Tables 10-12 in article [1] identify the hardening law, yield criterion and homogenization approaches. Fig. 2 summarizes where to find in [1]: the description of the numerous laws used (also reminded in Fig. 3), their identification and how results were presented. Finally, it points to some of the conclusions.

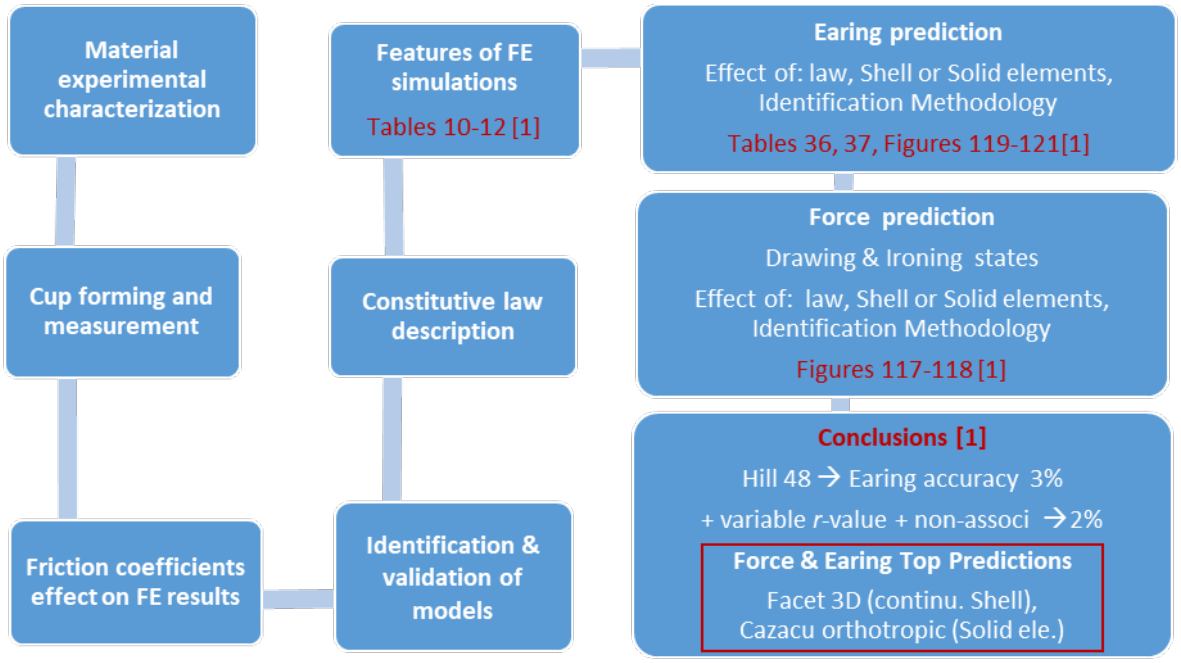

Fig. 2. Sections of article [1] describing the ESAFORM Benchmark 2021.

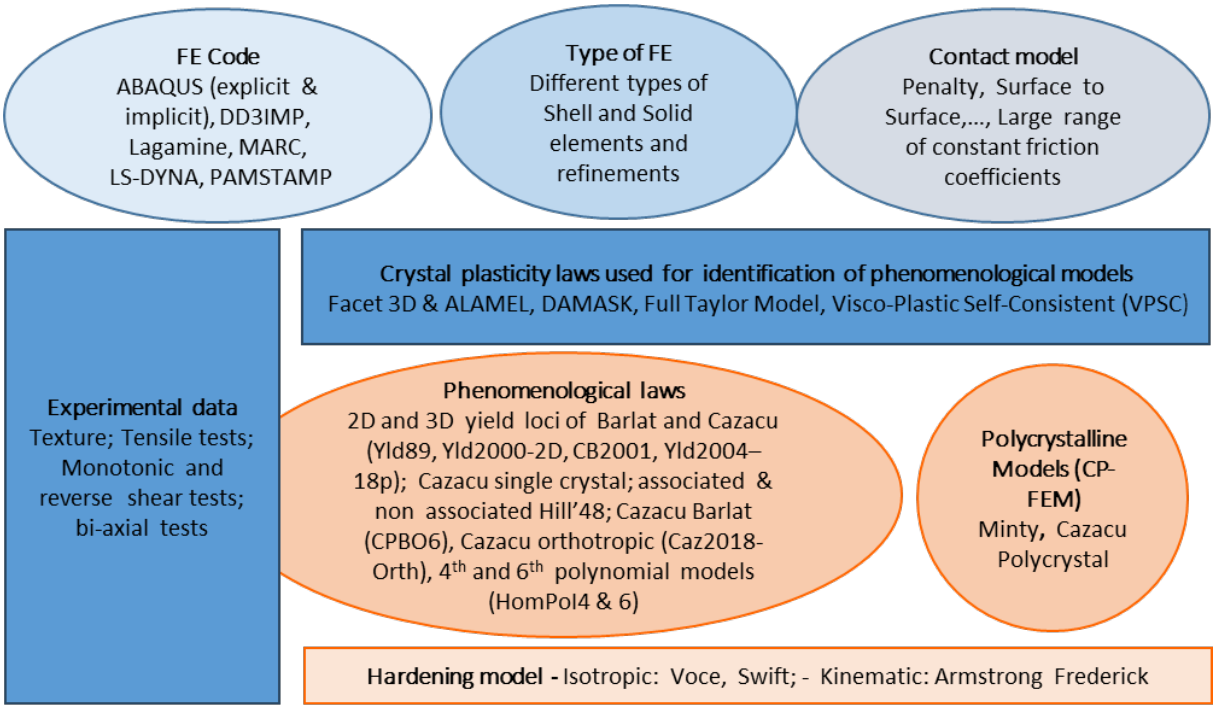

Fig. 3. Different model features involved in ESAFORM 2021 Benchmark: light blues define the FE codes, elements, contact models, while pink color points the constitutive laws used and dark blue rectangles explain how they are identified.

Fig. 3 summarizes all the material models used. An extensive discussion on model identification is provided in [1]. Here we just mention that for crystal plasticity models (CPM), it was detailed: i) the choice of the set of representative grains to model the texture; ii) the detailed methodology for identification of the parameters of the CPM; with tables for all parameter values, iii) predictions of Lankford coefficient variation and yield stress variation (see a summary in Fig. 4.). For both classical and recent anisotropic yield functions, the data set used for identification was either based on physical tests or on virtual tests computed with CPM, as synthesized in Fig. 5.

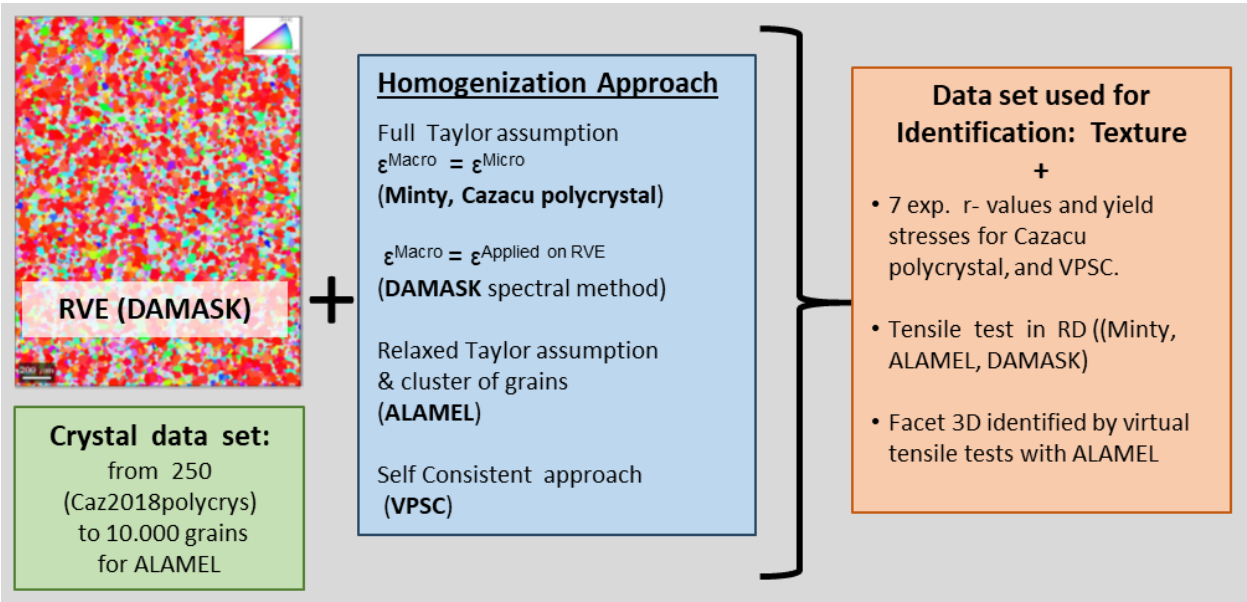

Fig. 4. Identification methodology and main homogenization schemes of the CPM.

Mechanical tests	Tensile	Lankford 0° 45° 90°	Yield stress 0°	Yield stress 45° 90°	Yield 15° 30° 60° 75°	Bi-axial =	Bi-axial ≠	Shear
Identification based on experiments - Phenomenological law	UCoimbra Hill48(A)							
	USakarya Yld89							
	REEF Caz2018-Orth - ULiege Hill48(A) - USakarya HomPol 4 & 6							
	UGent Yld200-2D*, POSTECH Yld200-2D & Yld2004-18p, NTNU Yld2004-18p*							
	UCoimbra CB2001							
	UAalto Hill48 (NA)							
	UCoimbra CPBO6 ex2							

Fig. 5. List of mechanical physical or virtual (CPM) tests used for the identification of the anisotropic yield functions used by the participants (see [1] for more details).*

To check the validity of the parameter identification of the anisotropic yield functions and respective CPM models, the participants had to provide the predicted in-plane evolutions for the Lankford coefficients and the yield stresses, for tensile directions varying from 0° to 90° to the RD. Cup drawing simulation results were discussed in detail in several subsections. First the FE results (solid and shell FE simulations) obtained using anisotropic yield functions, identified either from physical or virtual tests, and then FE results of cup drawing obtained with polycrystalline model results. It can be concluded that Hill48 provides satisfactory earing results (within 3% of earing measurements, see Fig.2); small differences in results obtained with Hill48, between various teams, due to FE modelling features. An overestimation of the ironing force was observed when using shell elements. Various possible improvements using a non-associated flow rule or variable Lankford coefficients were also discussed. Two models provided very accurate results for both earing and force: Facet 3D constitutive law [2], with continuum shell elements and identification based on CPM; and Cazacu orthotropic law [3], with solid elements and an identification relying on the 7 available physical tensile tests. The reader is referred to [1] for more details.

Influence of the Tool Stiffness

A part of the EXACT benchmark reported data was the measurement of the thickness at the top of the cup. It was roughly 0.1 mm larger than the gap between the punch and the die. Explanations were sought and discussed, one being that the gap was slightly bigger than initially reported, i.e., enough to justify the measured values. However, the geometry for the EXACT benchmark was done very carefully (see [1]), which did not support this assumption.

Here, we discuss further investigations done to provide explanations for attaining a cup with a thickness higher than the gap between the punch and the die. This could be related with the elastic deformation of the tools during the process. Note that the modelling of the tool deformation can be performed using different approaches, namely by adjusting the stiffness of the surfaces that describe the tool or modelling them as deformable bodies. The latter approach was adopted and simulations were conducted with the academic code DD3IMP, considering the Swift law and the Hill48 yield criterion, with the parameters provided by the benchmark committee. A friction coefficient of 0.06 was assumed between the blank and the tools, to improve the description of the drawing force. More details concerning the constitutive model and the friction coefficient adopted are presented in Table 1 (column Def1). For reference, simulations were performed considering rigid tools (Rig1 results).

Materials Research Proceedings 28 (2023) 1491-1502 https://doi.org/10.21741/9781644902479-161

Table 1. FE code, tool modelling approach, type of finite element for the blank, constitutive model and friction coefficient adopted in each model.

	Rig1	Rig2	Rig3	Def1	Def2	Def3
Software	DD3IMP	PAMStamp	Abaqus	DD3IMP	PAMStamp	AutoForm
Forming tools	Rigid	Rigid	Rigid	Deformable	Deformable	Deformable
Finite elements: type	Solid	Solid	Solid-Shell	Solid	Solid	Solid-Shell
and number	15408	55560	9743**	23313	171405	9390***
Hardening law	Swift	Swift	Swift	Swift	Swift	Swift
Yield criterion	Hill48	Hill48	Facet-3D	Hill48	Hill48	Facet-3D
Friction coefficient	0.06	0.075	0.09	0.06	0.075	0.09
CPU time*	3h02m	3h33m	2h46m	16h04m	37h48m	1h18m

* Note that different meshes (blank and tools) and CPUs were used with different codes; ** 5 through thickness integration points; *** 11 through thickness integration points

A similar approach was adopted at University of Siegen (USiegen) and simulations were conducted using the commercial code PAMStamp considering also hexahedral solid elements and the same constitutive model. The results were compared with those obtained with rigid tools, which were presented in [1]. To be noted that with rigid tools, a slightly higher value for the friction coefficient was considered, to capture the maximum punch force in the drawing stage in [1]. The model with deformable tools uses the same value such as to allow for direct comparison, as shown in Table 1 (Rig 2 and Def2).

In ESAFORM 2021 benchmark, the use of Facet-3D yield function with Abaqus/Explicit led to an accurate cup height profile and punch force curves. However, the thickness measured at different height sections was underestimated. In the follow up research, Facet-3D was used in AutoForm R10, since it allows implementing a user material and enables a convenient adjustment of the tool stiffness. In this work, the value of 10 GPa/mm was used for the punch, while for the die and the blank holder a higher value of 60 GPa/mm was adopted. This combination was found by trial and error to somehow trade-off the ironing force and the thickness distribution. With lower tool stiffnesses, the maximum sheet thickness increases and the ironing force decreases. Other details about these models are presented in Table 1 (Rig3 and Def3).

Fig. 6 (a) presents the comparison of the punch force evolution with its displacement, obtained with the different models, as well as the experimental results. Globally, the adoption of rigid or deformable tools has a negligible impact on the drawing stage, where the maximum value attained is mainly dictated by the value of the friction coefficient. Nevertheless, the maximum value of the ironing force drops when adopting deformable tools and solid elements for the blank. When the blank is discretized with solid-shell elements, the model with deformable tools shows a slight increase of the ironing force, but these results are not directly comparable, because different codes were used. Regarding the earing profile, although models Rig1 and Rig2 present quite similar average height and trend (see Fig. 6 (b)), the effect of considering deformable tools leads to a lower cup height for Def1, while for Def2 it increases. On the other hand, for the models adopting solid-shell elements the impact of considering deformable tools is negligible (Rig3 and Def3). Note that in this case the earing profile is not symmetric, because the initial position of the blank was off set, to improve the comparison with the experimental results [1].

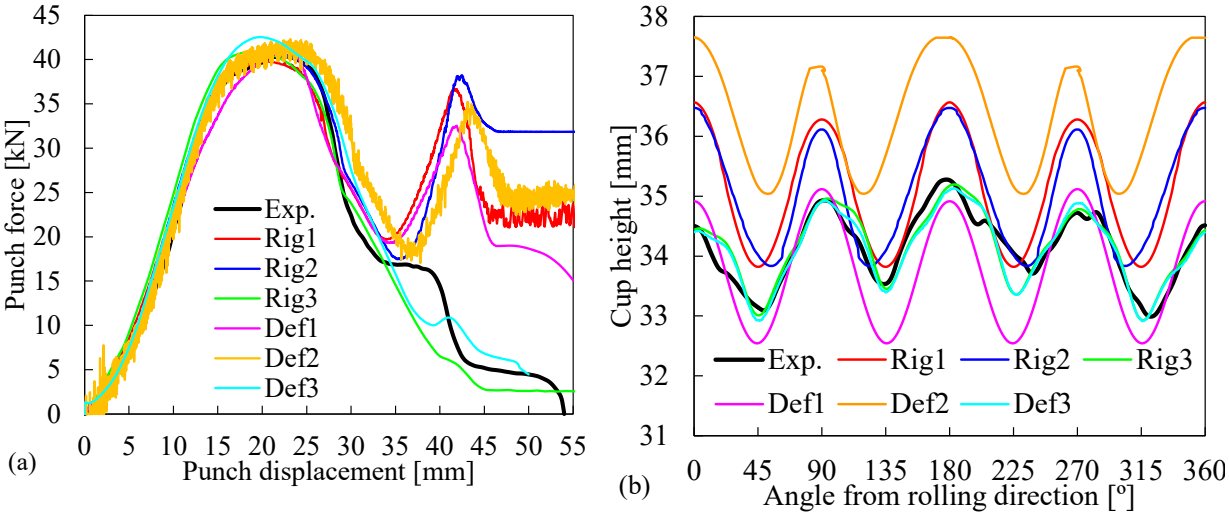

Fig. 6. Comparison between experimental and predicted results using rigid and deformable tools: (a) punch force-displacement and (b) earing profile.

The thickness distribution along the circumferential direction is presented in Fig. 7, for two values of cup height, 20 mm and 30 mm. The models that use rigid tools and solid elements (Rig 1 and Rig2) led to a trend like the experimental one for the lower height. For the higher height, the thickness is constant and equal to the value of the gap (1.2 mm) for Rig 1 while Rig2 predicts a slightly higher value, which indicates that the contact algorithm implemented in DD3IMP imposes the contact constraints more strictly. When adopting deformable tools, the models that use solid elements present different trends, with Def1 leading to higher thickness values for both heights, while Def2 underestimates the thickness value for both heights. These results seem to be coherent with the average cup height because lower thickness values result in a higher cup and *vice-versa* (see Fig. 6 (b)). Although the results are not directly comparable for solid-shell elements (Rig3 and Def3), one can see that the thickness estimation improves when considering deformable tools. In brief, deformable tools lead to thickness values on the top of the cup higher than the gap between the die and the punch, like in the experiment. In this context, it should be mentioned that the option of adjusting the stiffness of the surfaces has a negligible impact on the CPU time, when compared with the use of solid deformable tools (see Table 1).

The lower punch force value predicted for the ironing stage when adopting solid-shell elements had already been reported in [1]. The differences observed in the models obtained with solid elements and deformable tools seem to be related with distinction features in the treatment of the contact conditions. In fact, although not shown here, it was observed that the adoption of the penalty algorithm instead of the hard contact one, adopted in this work for PAMStamp, would lead to a clearly lower value for the force during the ironing stage. Thus, even when adopting deformable tools, an evolutional friction law is suggested to capture the drawing and the ironing forces in a more realistic way [4]. In this context, some of the authors are working on an improved analysis of the contact conditions, considering the experimental analysis of the contact conditions using flat strip drawing friction tests.

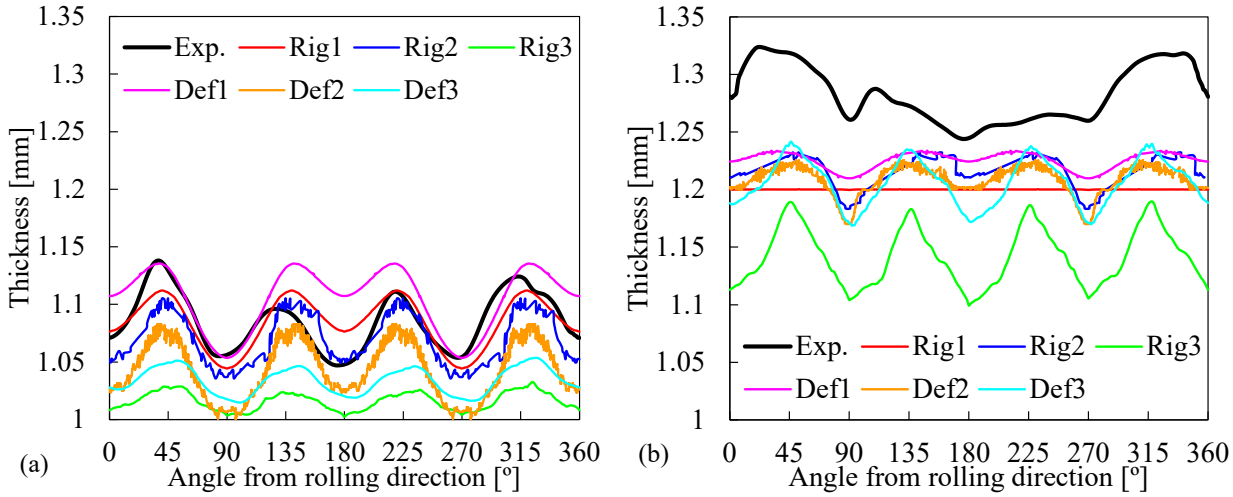

Fig. 7. Comparison between experimental and numerical wall thickness distribution along the circumferential direction evaluated at different cup height values: (a) H=20 mm; (b) H=30 mm.

CP-Based and Phenomenological Modelling of Kinematic Hardening Behavior

The experimental cyclic shear deformation behavior of AA 6016-T4 sheet, observed in Fig.12 of [1] and reported in Fig. 8 (b) hereafter, presents a kinematic hardening phenomenon. To capture this phenomenon, a two-surface model was proposed by Yoshida and Uemori (YU) and has been widely used in sheet metal forming analysis [5-6]. It consists of a yield surface and a bounding surface, in which the kinematic hardening is described by moving the yield surface within the bounding surface. Hereafter, an associated flow rule (AFR) based two-surface hardening model is proposed, which is modified from the non-AFR based two-surface model proposed by Ghaei et al. [7]. The YU hardening model was incorporated with an advanced yield function to describe the complex deformation behavior in sheet metal forming. In this model, the yield criterion f_y determines the boundary between the elastic and plastic zone using the yield stress y in the stress space and the function $\boldsymbol{F}$ determines the shape of the bounding surface, as given by:

$$f_y(\boldsymbol{\eta}) - y = 0 \tag{1}$$

$$F(\boldsymbol{\Sigma} - \boldsymbol{\alpha_2}) - b_0 - r(p) = 0$$

$$\boldsymbol{\eta} = \boldsymbol{\sigma} - \boldsymbol{\alpha}$$

where $\boldsymbol{\sigma}$ is the Cauchy stress tensor in current state, $\boldsymbol{\Sigma}$ is the stress tensor corresponding to the bounding surface, and $\boldsymbol{\alpha}$ is the backstress tensor controlling the movement of the yield surface. $\boldsymbol{\eta}$ is substituted into the yield criterion to calculate the effective stress. $\boldsymbol{\alpha_2}$ is the corresponding backstress tensor and b_0 is the initial size of the bounding surface. r controls the expansion of the bounding surface, which is governed by the equivalent plastic strain p:

$$r(p) = Q[1 - \exp(-bp)] \tag{2}$$

where the Q and b are the material constants that need to be calibrated. In this model, the kinematic hardening behaviour is governed by the state of the backstress $\boldsymbol{\alpha}$, which can be decomposed as $\dot{\boldsymbol{\alpha}} = \dot{\boldsymbol{\alpha}}_1 + \dot{\boldsymbol{\alpha}}_2$. $\dot{\boldsymbol{\alpha}}_1$ is dependent on the rate of equivalent plastic strain $\dot{p}$, and can be described by:

$$\dot{\boldsymbol{\alpha}}_1 = \gamma_1 \left(\frac{b_0 + r - y}{y} \boldsymbol{\eta} - \boldsymbol{\alpha_1} \right) \dot{p} \tag{3}$$

where γ_1 is the material constant. $\boldsymbol{\alpha_1}$ is the deviation between the central position of the yield surface and the bounding surface, whose motion is controlled through $\dot{\boldsymbol{\alpha}}_2$, as given by:

$$\dot{\boldsymbol{\alpha}}_2 = \gamma_2 \left(\frac{c_2}{y} \boldsymbol{\eta} - \boldsymbol{\alpha_2} \right) \dot{p} \tag{4}$$

where c_2 and γ_2 are the material parameters. $\boldsymbol{\alpha_2}$ is the central position of the bounding surface in the stress space. To obtain the equivalent plastic strain rate $\dot{p}$, the classical AFR is employed:

$$\dot{\boldsymbol{\epsilon}}^{\boldsymbol{p}} = \dot{\lambda} \frac{\partial f_y}{\partial \boldsymbol{\sigma}} = \dot{\lambda} \boldsymbol{m} \tag{5}$$

where $\dot{\boldsymbol{\epsilon}}^{\boldsymbol{p}}$ is the rate of the plastic strain tensor and $\dot{\lambda}$ is the plastic multiplier, which is equal to the equivalent plastic strain rate in AFR, i.e., $\dot{p} = \dot{\lambda} \boldsymbol{m}$ is the first order of the yield function, which makes the plastic potentials normal to the yield surface. A consistency condition in the yield surface and bounding surface is utilized to solve the equivalent plastic strain rate:

$$\frac{\partial f_y}{\partial \boldsymbol{\sigma}} : \dot{\boldsymbol{\sigma}} + \frac{\partial f_y}{\partial \boldsymbol{\alpha_1}} : \dot{\boldsymbol{\sigma}}_1 + \frac{\partial f_y}{\partial \boldsymbol{\alpha_2}} : \dot{\boldsymbol{\sigma}}_2 = \boldsymbol{m} : \dot{\boldsymbol{\eta}} = 0 \tag{6}$$

Here, the elastic stress tensor follows Hooke's law, and hence the rate of the stress tensor is obtained by:

$$\dot{\boldsymbol{\sigma}} = \boldsymbol{D} : \left(\dot{\boldsymbol{\epsilon}} - \dot{\boldsymbol{\epsilon}}^{\boldsymbol{p}} \right) = \boldsymbol{D} : \left(\dot{\boldsymbol{\epsilon}} - \dot{\lambda} \boldsymbol{m} \right) \tag{7}$$

where $\boldsymbol{D}$ is the elastic stiffness matrix, and $\dot{\boldsymbol{\epsilon}}$ is the rate of the total strain tensor. The plastic multiplier can thus be represented by:

$$\boldsymbol{m} : \boldsymbol{D} : \left(\dot{\boldsymbol{\epsilon}} - \dot{\lambda} \boldsymbol{m} \right) - \boldsymbol{m} : \dot{\boldsymbol{\alpha}}_1 - \boldsymbol{m} : \dot{\boldsymbol{\alpha}}_2 = 0 \tag{8}$$

Therefore, the plastic multiplier (equivalent plastic strain rate) can be obtained:

$$\dot{p} = \frac{\boldsymbol{m} : \boldsymbol{D} : \dot{\boldsymbol{\epsilon}}}{\boldsymbol{m} : \boldsymbol{D} : \boldsymbol{m} + \boldsymbol{m} : \frac{\dot{\boldsymbol{\alpha}}_1}{\dot{p}} + \boldsymbol{m} : \frac{\dot{\boldsymbol{\alpha}}_2}{\dot{p}}} \tag{9}$$

In addition, the tangent consistent modulus $\boldsymbol{D^{ep}}$ of the two-surface hardening model is determined:

$$\dot{\boldsymbol{\sigma}} = \boldsymbol{D^{ep}} : \dot{\boldsymbol{\epsilon}} = \left(\boldsymbol{D} - \frac{(\boldsymbol{D} : \boldsymbol{m}) \otimes (\boldsymbol{D} : \boldsymbol{m})}{\boldsymbol{m} : \boldsymbol{D} : \boldsymbol{m} + \boldsymbol{m} : \frac{\dot{\boldsymbol{\alpha}}_1}{\dot{p}} + \boldsymbol{m} : \frac{\dot{\boldsymbol{\alpha}}_2}{\dot{p}}} \right) \tag{10}$$

Besides the permanent softening, workhardening stagnation is observed at the early stage of reverse loading [5]. To describe this phenomenon, a stagnation surface is introduced to limit the expansion of the bounding surface. In this method, the expansion of the bounding surface is only

Materials Research Proceedings 28 (2023) 1491-1502 https://doi.org/10.21741/9781644902479-161

allowed when the central position of the bounding surface is within the range of the stagnation surface. This stagnation surface is given as follows:

$$f_s(\boldsymbol{\alpha_2} - \boldsymbol{\alpha_s}) - y_s = 0 \tag{11}$$

where y_s and $\boldsymbol{\alpha_s}$ are the initial size and the central location of the stagnation surface in stress space, respectively. A non-linear kinematic hardening law is utilized to describe the translation of the bounding surface:

$$\dot{\boldsymbol{\alpha}}_s = \dot{\mu}(\boldsymbol{\alpha_2} - \boldsymbol{\alpha_s}) = \dot{\mu}\boldsymbol{\xi} \tag{12}$$

where the tensor $\boldsymbol{\xi}$ and rate $\dot{\mu}$ are achieved using the following criterion:

$$\frac{\partial f_s}{\partial \boldsymbol{\alpha_2}} : \dot{\boldsymbol{\alpha}}_2 + \frac{\partial f_s}{\partial \boldsymbol{\alpha_s}} : \dot{\boldsymbol{\alpha}}_s - \dot{y}_s = 0 \tag{13}$$

where the $\dot{\mu}$ is obtained by,

$$\dot{\mu} = \frac{\boldsymbol{n} : \dot{\boldsymbol{\alpha}}_2 - \dot{y}_s}{\boldsymbol{n} : (\boldsymbol{\alpha_2} - \boldsymbol{\alpha_s})} \tag{14}$$

where $\boldsymbol{n} = \frac{\partial f_s}{\partial \boldsymbol{\alpha_2}}$. The rate of y_s is defined as:

$$\begin{cases} \dot{y}_s = h\boldsymbol{n} : \dot{\boldsymbol{\alpha}}_2, & when \quad \dot{r} > 0 \\ \dot{y}_s = 0, & when \quad \dot{r} = 0 \end{cases} \tag{15}$$

where h is the calibrated material constant, which controls the expansion level of the stagnation surface. The $\dot{r}$ determines that the stagnation surface is only allowed to expand associated with the expansion of the bounding surface.

Kinematic hardening model calibration and validation was based on the results of DAMASK solver, a CPM model (see [1] Norwegian University of Science and Technology (NTNU) participant approach) used to predict the stress response of AA6016-T4 during the cyclic deformation. The parameters of the modified YU kinematic hardening model are identified with a virtual uniaxial tension-compression test in RD (1.5 cycles), as given in Table 2. To evaluate the performance of the calibrated hardening model at various strain levels, a comparison between the stress-strain curves predicted by CPM simulation and YU model for five tension-compression cycles was illustrated in Fig. 8 (a). It was found that the calibrated YU hardening model can well capture the tension-compression full-CPM history stress-strain response. Fig. 8 (b) shows that the modified YU model identified by the virtual uniaxial tension-compression tests coupled with Yld2004-18p yield function is capable of accurately predicting the experimental mechanical response of AA6016-T4 in the shear-reverse shear deformation mode measured in [1].

Table 2. The parameters of the modified two-surface kinematic model for the AA6016-T4 sheet.

y(MPa)	b_0(MPa)	γ_1	c_2(MPa)	γ_2	Q(MPa)	b	h
101.2	105.3	850	25.2	391.3	158.3	12.8	0.18

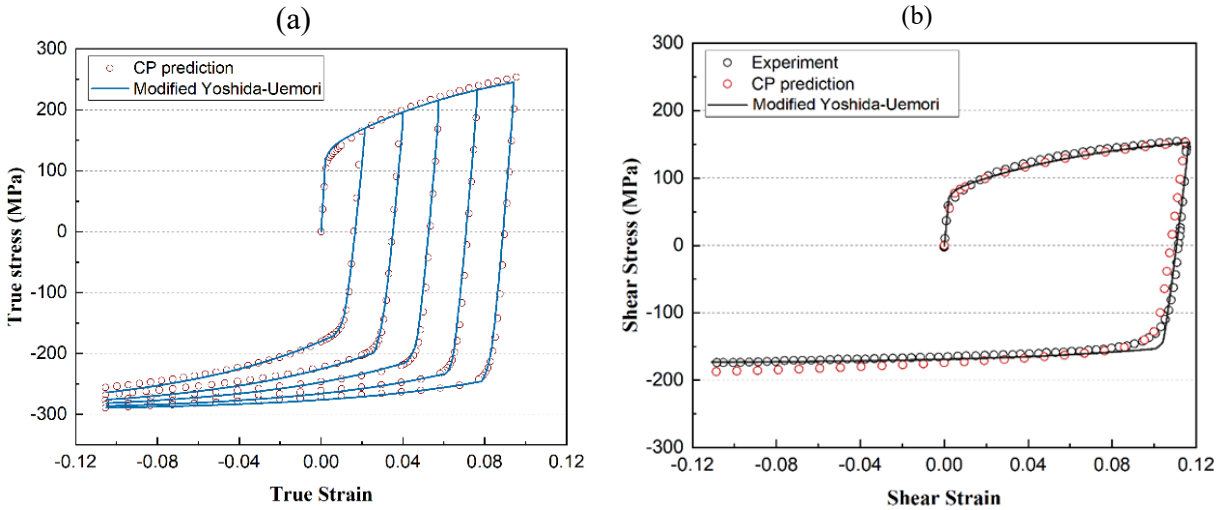

Fig. 8. (a) Comparison of stress-strain response of 5 tension-compression cycles by CPM simulations and modified YU model. (b) comparison of shear-reverse shear stress-strain responses from experiment [1], DAMASK CPM predictions, results of Yld2004-18p yield function coupled with modified YU model.

Summary

The ESAFORM Benchmark series is an ongoing adventure (https://esaform.org/grants/), do not hesitate to apply. It allows a whole community to exchange ideas about an issue that poses difficulties to realize reliable and efficient forming processes and, or simulations.

In 2021 cup drawing benchmark, the simulations pointed out that phenomenological laws identified using only physical experiments or completed by crystal plasticity results could reach accurate predictions of force evolution, final earing and thickness distribution. Additionally, an issue about the ironing force, the wall thickness distribution and the punch-die gap drew attention to the question of friction and tool elasticity. The current article demonstrates that both effects are important and it suggests that a variable friction parameter could be required to improve ironing force prediction. Nevertheless, even with a single tuned friction coefficient, the Facet 3D model, considering the tool deformation available in AutoForm R10 was able to improve its thickness prediction accuracy at the top of the cup compared to its results based on rigid tools. Models with rigid and deformable tools, built in DD3IMP and PAMStamp, led to physically consistent results, coherent with the experimental ones.

The extensive experimental results gathered in [1] allow the identification of advanced anisotropic elastoplastic models, as shown by the work of NTNU and Northwestern Polytechnical University (Taican, China), with their advanced two-surface model. Validated on experimental reverse shear tests, pointing the need of an accurate kinematic behaviour model, their work is still ongoing to present a cup deep drawing application.

The reader can consult the open access article [1] for a more detailed analysis of all the benchmark results and access to the data (https://zenodo.org/record/6874577#.Y4YhzHbMKyA).

References

[1] A.M. Habraken, T.A. Aksen, J.L. Alves, R.L. Amaral, E. Betaieb, N.Chandola, L. Corallo, D.J. Cruz, L. Duchêne, B. Engel, E. Esener, M. Firat, P. Frohn-Sorensen, J. Galan-Lopez, H. Ghiabakloo, L.A.I. Kestens, J. Lian, R. Lingam, W. Liu, Jun Ma, L.F. Menezes, T.Nguyen-Min, S.S. Miranda, D.M. Neto, A.F.G. Pereira, P.A. Prates, J. Reuter, B. Revil-Baudard, C. Rojas-Ulloa, B. Sener, F. Shen, A. Van Bael, P. Verleysen, F. Barlat, O. Cazacu, T. Kuwabara, A. Lopes, M.C. Oliveira, A.D. Santos, G. Vincze, Analysis of ESAFORM 2021 cup drawing benchmark of an Al alloy, critical factors for accuracy and efficiency of FE simulations, Int. J. Mater. Form. 15 (2022) 61. https://doi.org/10.1007/s12289-022-01672-w

[2] P. Van Houtte, S.K. Yerra, A. Van Bael, The facet method: a hierarchical multilevel modelling scheme for anisotropic convex plastic potentials, Int. J. Plast. 25 (2009) 332-360. https://doi.org/10. 1016/j.ijplas.2008.02.001

[3] O. Cazacu, New yield criteria for isotropic and textured metallic materials, Int. J. Solids Struct. 139 (2018) 200-210. https://doi.org/10.1016/j.ijsolstr.2018.01.036

[4] M.C. Oliveira, D.M. Neto, A.F.G. Pereira, J.L. Alves, L.F. Menezes, Evaluating the influence of the deformation of the forming tools in the thickness distribution along the wall of a cylindrical cup, IOP Conf. Series: Mate. Sci. Eng. 1238 (2022) 012079. https://doi.org/10.1088/1757-899X/1238/1/012079

[5] F. Yoshida, T. Uemori, A model of large-strain cyclic plasticity describing the Bauschinger effect and workhardening stagnation, Int. J. Plast. 18 (2002) 661-686. https://doi.org/10.1016/S0749-6419(01)00050-X

[6] F. Yoshida, H. Hamasaki, T. Uemori, Modeling of anisotropic hardening of sheet metals including description of the Bauschinger effect, Int. J. Plast. 75 (2015) 170-188. https://doi.org/10.1016/j.ijplas.2015.02.004

[7] A. Ghaei, A. Taherizadeh, A two-surface hardening plasticity model based on non-associated flow rule for anisotropic metals subjected to cyclic loading, Int. J. Mech. Sci. 92 (2015) 24-34. https://doi.org/10.1016/j.ijmecsci.2014.11.017